Mon. Not. R. Astron. Soc. **355,** 31–36 (2004) doi:10.1111/j.1365-2966.2004.08286.x

Radio and X-ray observations of PSR B0540–69

Simon Johnston,[1⋆] Roger W. Romani,[2] F. E. Marshall[3] and W. Zhang[3]

[1]*School of Physics, University of Sydney, NSW 2006, Australia*
[2]*Department of Physics, Stanford University, Stanford, CA 94305-4060, USA*
[3]*Laboratory for High-energy Astrophysics, Goddard Space Flight Center, Greenbelt, MD 20771, USA*

Accepted 2004 August 4. Received 2004 August 2; in original form 2004 May 25

ABSTRACT

PSR B0540−69 is one of a small handful of pulsars known to emit giant pulses and the only extra-galactic pulsar known to do so. We observed the pulsar for a total of 72 h over a 6 month interval and detected 141 giant pulses. We have obtained correct phasing between the radio arrival times of the giant pulses and the X-ray pulse profile. The giant pulses occur in two phase windows, located 6.7 ms before and 5.0 ms after the mid-point of the X-ray profile. We have detected the integrated profile of the pulsar at 1.4 GHz with a flux density of only 24 μJy. The statistics of the giant pulses are clearly power law and it is likely that the giant pulses contribute only a few per cent of the integrated pulse flux density, similar to other pulsars with giant pulse emission. Simultaneous X-ray and radio observations show no significant increase in the X-ray flux at the time of the radio giants. The relative enhancements in the X-ray emission must be at least 5.5 times smaller than in the radio emission.

Key words: pulsars: individual: PSR B0540−69.

1 INTRODUCTION

PSR B0540−69 was discovered in the early 1980s by Seward, Harnden & Helfand (1984) using data from the Einstein X-ray Observatory. The pulsar is located inside the supernova remnant SNR 0540–693 in the Large Magellanic Cloud (LMC). It has a short rotation period (∼50 ms) and a rapid spin-down with a characteristic age of only 1500 yr. The X-ray profile of the pulsar consists of a single broad profile that covers approximately half the pulse phase (de Plaa, Kuiper & Hermsen 2003). The profile is not Gaussian in shape, but appears to be double peaked and also contains structure on the rising and trailing edges. The profile does not appear to evolve significantly from optical to hard X-rays. This pulse shape is in contrast to the high-energy emission from the Crab pulsar. In the Crab pulsar, two sharp peaks with a separation of 0.4 pulse phase are seen at all energies.

The radio emission from PSR B0540−69 went undetected for a decade until Manchester et al. (1993) discovered a broad, weak radio pulse at 0.64 GHz. The flux density at that frequency is 0.4 mJy and the pulse duty cycle is more than 80 per cent with a hint of a double profile, similar to the profile seen at high energies. Manchester et al. (1993) failed to detect the pulsar at either 1.4 or 0.44 GHz.

The pulsar was observed with the Parkes radio telescope in 2001 as part of a survey to detect giant pulses from young and millisecond pulsars. Single pulses were detected with energy more than 1000 times that of the average pulse energy (Johnston & Romani 2003; hereafter Paper I). Such strong pulses, first seen in the Crab pulsar, are called 'giant pulses' and this was their first detection from an extra-galactic pulsar. The giant pulses are scatter broadened at 1.4 GHz with an exponential scattering time of 0.4 ms and have an emission bandwidth of at least 256 MHz. There is some evidence that the flux density distribution of the giant pulses is a power law with a shallower index than those seen for the Crab pulsar and PSR B1937+21 (Paper I). In the Crab pulsar, PSR B1937+21 and PSR B1821–24 the giant pulses are exactly in phase with the high-energy emission, which provides evidence that their emission may have a common origin Romani & Johnston (2001). An attempt was made to match the phases of the radio giant pulses with the X-ray profile for PSR B0540−69 obtained with the *Rossi X-ray Timing Explorer* (*RXTE*), however, this was subject to caveats concerning the absolute timing between the X-ray and the radio emission, and, as shown later in this paper, was incorrect in Paper I. In 8 h of integration Johnston & Romani (2003) failed to detect any integrated flux density from the pulsar to a level of 13 μJy, assuming a duty cycle of 10 per cent. This implies the spectral index between 0.64 and 1.38 GHz must be steeper than −4.4.

Timing of the pulsar has been carried out in the X-ray band since its discovery. The two most recent papers dealing with the timing are Cusumano, Massaro & Mineo (2003a) and Zhang et al. (2001). In the latter paper, the authors found evidence for a glitch in the pulsar, however, Cusumano et al. (2003a) ascribe this to timing noise. The main result of the timing of this pulsar is that the pulsar braking index is substantially less than the value of 3.0 expected from pure magnetic dipole spin-down. The actual value of the braking index is subject to some uncertainty and ranges from 1.8 to 2.8 depending on the data set used.

⋆E-mail: simonj@physics.usyd.edu.au

Simultaneous searches for giant pulse emission at radio and high energies have been made towards the Crab pulsar. Lundgren et al. (1995) observed with OSSE in the 50–220 keV band and in the radio band. They detected no enhanced emission at high energies and concluded that the γ-ray enhancement is a factor of 10 less than in the radio band. More recently, Shearer et al. (2003) reported a small increase in the optical flux of the Crab pulsar coincident with the giant pulses in the radio band. However, the optical enhancement is 700 times less than seen in the radio band. Both Vivekanand (2001a,b) and Cusumano et al. (2003b) report on long *RXTE* observations of the Crab pulsar and PSR B1937+21, respectively, and reported limits on X-ray enhancements at least 640 and 230 times less than expected from equivalent duration radio observations.

In this paper we report on further radio observations of PSR B0540−69. We obtained simultaneous X-ray and radio observations on 2003 August 6 and September 28. In conjunction with data from the Crab pulsar, this has allowed us to directly compare the phase of the X-ray profile with the radio giants. This is described in detail in Section 3. In Section 4 we discuss the location and statistics of the giant radio pulses, and in Section 5 we report on the detection of the integrated profile of the pulsar. We conclude with some comments on the implications for the location and mechanism of the magnetospheric process generating the giant pulse emission.

2 OBSERVATIONS

All the radio observations of PSR B0540−69 were made with the 64-m Parkes radio telescope. We used the centre beam of the 21-cm multibeam receiver at an observing frequency of 1390 MHz. The receiver had a system equivalent flux density of 27 Jy on cold sky. The back-end consisted of a filter-bank system containing 512 channels per polarization, each of width 0.5 MHz for a total bandwidth of 256 MHz. The polarization pairs were summed to form the total power, each output was then sampled at 80 μs, one-bit digitized, and written to DLT for off-line analysis. Table 1 lists the observation dates for the pulsar, including the initial observations in 2001. The final column of the table gives the time on source during the observing session. The total observing time for the 2003 sessions was 71.5 h. During the 2003 August and September observing sessions the Crab pulsar was observed on each day for 20 min. The integration time is sufficient to detect the integrated profile of the Crab pulsar and a number of giant pulses. This provides us with a check both for the software detection algorithm used in detecting giant pulses and for the absolute timing between the Parkes telescope and the *RXTE* satellite.

In the off-line analysis the data were dedispersed using a dispersion measure (DM) of 146.5 cm^{-3} pc (Paper I) to produce an output stream of 80-μs time samples. Data showing strong interference were clipped, and the data set searched for giant pulses exceeding some threshold using the technique described in Paper I. For this part of the analysis, the absolute phase of each time sample is not important.

In order to produce the integrated pulse profile, and to determine the phase of the giant pulses, an accurate radio ephemeris was first derived using standard timing techniques. Then, each time sample could be tagged with an appropriate pulse rotation phase. These samples were summed to form an integrated profile with a maximum of 630 phase bins per period.

X-ray observations are obtained using *RXTE*. PSR B0540−69 is observed regularly (∼40 times per year) along with the other young LMC pulsar J0537−6910 as part of a monitoring programme (Zhang et al. 2001), as is the Crab pulsar. X-ray arrival times are obtained from 3- to 20-keV PCA data, using pulse height channels 5–50 from the top layer of the detector. After fitting to a sinusoidal template, these data provide arrival times with an accuracy of ∼0.4 ms relative to UTC. We used observations of the Crab pulsar taken near the epoch of the PSR B0540−69 observations to cross-check the Parkes–*RXTE* timing (see Section 3.1 below).

Table 1. Log for the radio observations of PSR B0540−69.

Date range	MJD range	Time (h)
2001 May 20–22	52 049–52 051	8.5
2003 May 17–18	52 776–52 777	6.8
2003 May 24–25	52 783–52 784	9.7
2003 June 3	52 793	4.3
2003 August 4–10	52 855–52 861	31.2
2003 September 7–8	52 889–52 890	10.3
2003 September 24–28	52 906–52 910	9.2

3 X-RAY AND RADIO TIMING

3.1 Crab pulsar

In order to compare the absolute phasing between the *RXTE* X-ray observations and the Parkes radio observations, we first used data taken on the Crab pulsar. The Crab pulsar was observed with *RXTE* on 2003 August 4 and the arrival time of the main pulse at infinite frequency at the barycentre occurred 10 938.056 463 66 s after MJD 528 55.0. At Parkes, observations of the Crab pulsar were made on 2003 August 4 and 7–9. Each observation was 20 min in duration at a frequency of 1390 MHz and the sampling rate was 80 μs. Topocentric arrival times at 1390 MHz were recorded for the ∼20 largest giant pulses in each of the observations. We also made use of the Jodrell Bank timing data on the Crab pulsar, in particular the published barycentric arrival times on 2003 June 15, July 15 and August 15.

The Jodrell Bank ephemeris for 2003 July 15 was used initially. This gives a rotation frequency of 29.804 428 6490 Hz, a frequency derivative of $-3.735\,3779 \times 10^{-10}$ and a DM of 56.76 cm^{-3} pc. The standard timing package, TEMPO, was used with this ephemeris and the arrival times for *RXTE*, Jodrell Bank and Parkes data as described above. The resultant residual is shown in the top panel of Fig. 1. We then fitted for frequency, frequency derivative and frequency second derivative, and the residual from this fit is shown in the lower panel of the figure. It can be seen that all three data sets agree within the errors and the radio giants have a relatively large jitter in their arrival times. We therefore believe that the times of arrival (TOA) of the *RXTE* data are correct within the quoted errors and that the Parkes data are correctly dedispersed and time tagged.

3.2 PSR B0540−69

Each data set on PSR B0540−69 was searched for giant pulses and their topocentic time of arrival at 1390 MHz was recorded with an accuracy of 80 μs. As shown in Paper I, the giant pulses in PSR B0540−69 occur in two groups separated by approximately 0.25 phase (12 ms). Within each group the jitter is 0.1 phase (5 ms).

Simultaneous *RXTE* and Parkes observations were made on 2003 August 6. The arrival of the X-ray pulse at the barycentre occurred 74 832.4986 s after MJD 528 57.0 and at this epoch the rotation

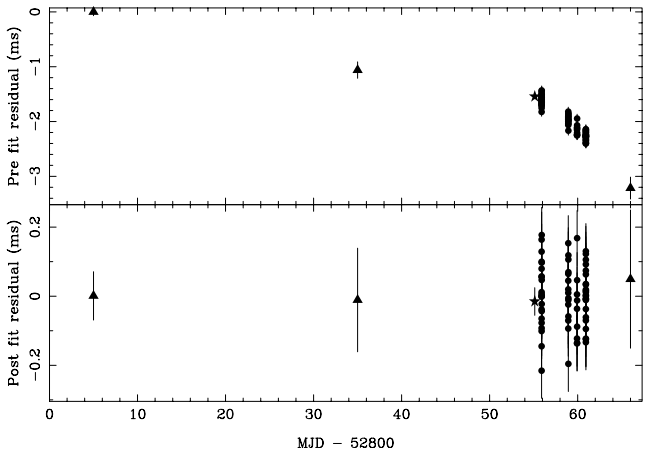

Figure 1. Pre-fitting (top panel) and post-fitting (bottom panel) residuals for the Crab pulsar from radio data taken at Jodrell Bank and Parkes and X-ray data from *RXTE*. The *RXTE* data point is marked with a star, the Jodrell Bank data are shown as triangles and the Parkes data are shown as dots.

frequency was 19.775 530 Hz. A second *RXTE* epoch was obtained on 2003 August 17. Using the rotation frequency of 19.775 350 Hz obtained on that date, we computed a frequency derivative of -1.87×10^{-10} s^{-2} between the two dates. This yielded an initial timing solution for the pulsar. We then included the times of arrival of the giant pulses detected during the August session. For timing purposes, we picked only the largest amplitude pulses so that the results would not be affected by possible spurious giants at low signal-to-noise ratios. We split the giants into the two groupings and timed each group separately. This allowed us to update the timing solution. We then added all the data obtained during the 130 d of observing the pulsar. At this point it was necessary to fit for the second frequency derivative. Finally, we also obtained the TOAs for all *RXTE* observations of the pulsar during 2003. We fitted the X-ray only data for the rotation frequency and the first two derivatives.

The timing solutions are given in Table 2. The pulsar position (obtained from optical measurements by Caraveo et al. 1992) and the DM (from Paper I) were held fixed in the fitting process. The errors are quoted in the last digit and are twice the formal errors given by the TEMPO software. The two groups of giants give the same results within the errors. The fitted parameters obtained from the X-ray data are largely consistent with the radio data. The frequency second derivative is the main difference, but this term is dominated by short-term timing noise in the radio band, which is averaged out in the longer X-ray data set. As part of the fitting process we can obtain the offset between the fiducial point of the X-ray profile and the mean location of the giants. The late giants arrive 5.0 ms after the X-rays and the early giants arrive 6.7 ms before the X-rays. The braking index is obtained from the spin frequency and the first two derivatives and is 2.36 for the X-ray data consistent with the previously known result.

Fig. 2 shows the residuals for the X-ray TOAs and the radio giant pulse TOAs compared with the model given by a fit to the X-ray data over a period of 300 d. In this plot, the triangles denote the X-ray timing points. Points at positive residuals denote the late arriving giants; those with negative residuals denote the early arriving giants.

4 STATISTICS OF THE GIANT PULSES

To highlight the relative phases of the X-ray and radio giants, we summed together the 18 largest giant pulses that occurred during the 2003 August observations. We define phase zero as the peak of the sinusoidal X-ray timing template, which in turn is related to the high-statistics, integrated *RXTE* profile of de Plaa et al. (2003) by a fit to the analytic decomposition of this profile. Together with the absolute timing between the radio and X-rays as described in Section 3, this analysis determines the relative phase to better than 1 ms ($\delta\,\phi = 0.02$). The two profiles are shown in Fig. 3 where it can be seen that the profiles are well aligned but the peaks of the giant pulse profile slightly lead the centroids of the corresponding X-ray pulse components. In fact, the sharp features on the X-ray peaks noted by de Plaa et al. (2003, at $\phi = 0.94$ and 0.04 in our figure) correspond somewhat better to the giant profile separation and phase.

For the data taken in 2003 August, we dedispersed the data at the DM of the pulsar, 146.5 cm^{-3} pc, and also at a DM of 125 cm^{-3} pc. We used the latter data as a check on the detection algorithm for the giant pulses as we should not have any giants at this DM. From this, we established a detection threshold of 4.5 mJy for the giant pulses. Fig. 4 shows the flux density of giant pulse candidates as a function of pulse phase for the data dedispersed at both 146.5 and 125 cm^{-3} pc. At a DM of 125 cm^{-3} pc only seven pulses were above the threshold (out of 2×10^6 pulses observed). At the correct DM of 146.5 cm^{-3} pc we see a concentration of giant pulses at two distinct phases.

Fig. 5 shows the flux density versus phase of all 141 giant pulses from the entire data set (top panel) and a histogram of location of the giant pulses as a function of pulse phase (bottom panel). Giant pulses seem to originate throughout the window from phases 0.78 to 1.18 although they are concentrated in two distinct peaks. There are 60 giant pulse candidates that arrive early (with respect to the X-ray

Table 2. Timing solutions for PSR B0540−69.

	Late giants	Early giants	X-ray
RA (J2000)	$05^h\,40^m\,11\overset{s}{.}22$	$05^h\,40^m\,11\overset{s}{.}22$	$05^h\,40^m\,11\overset{s}{.}22$
Dec. (J2000)	$-69^\circ\,19'\,54\overset{''}{.}98$	$-69^\circ\,19'\,54\overset{''}{.}98$	$-69^\circ\,19'\,54\overset{''}{.}98$
DM (cm^{-3} pc)	146.5	146.5	–
ν (s^{-1})	19.775 529 613(6)	19.775 529 618(6)	19.775 529 6113(8)
$\dot{\nu}(\times 10^{-12}s^{-2})$	−187.287(1)	−187.288(1)	−187.2853(4)
$\ddot{\nu}(\times 10^{-21}s^{-3})$	5.0(1.5)	4.3(1.3)	4.18(6)
Braking index, n	2.8(0.8)	2.4(0.7)	2.36(3)
Period epoch (MJD)	52 857.866	52 857.866	52 857.866
No TOAs	43	32	42
Rms residual (ms)	0.91	0.98	0.48
Arrival phase	0.10	0.87	0.00
Offset from X-ray (ms)	+5.0(0.3)	−6.7(0.3)	0.00

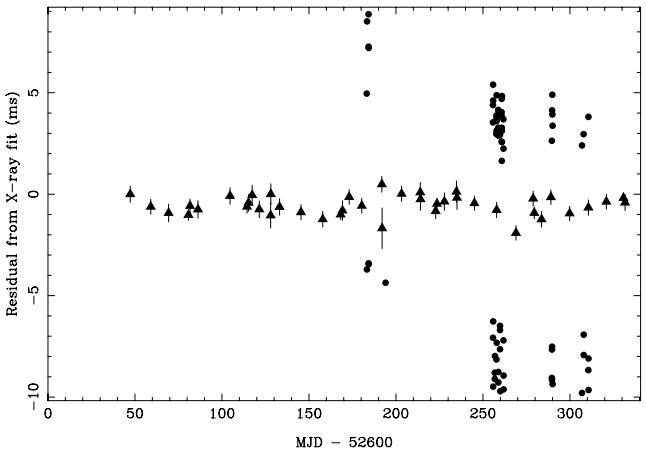

Figure 2. Timing residuals from the X-ray TOAs and giant pulse TOAs from PSR B0540−69 compared with the model given in the third column of Table 2. Triangles denote X-ray data and circles the radio data. The division into two clumps of giants can clearly be seen.

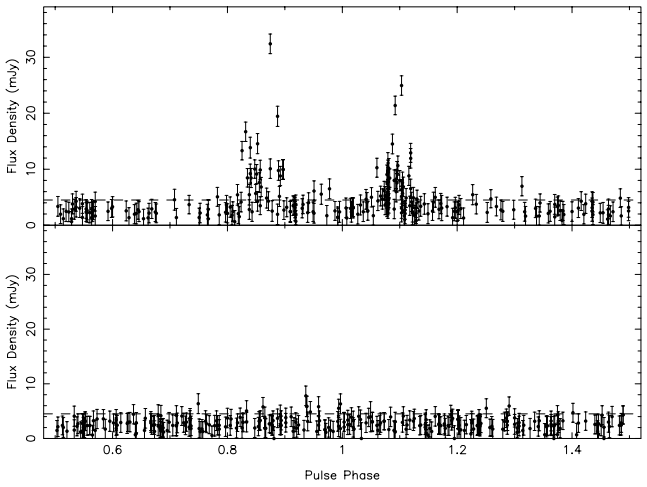

Figure 4. Location and amplitudes of giant pulses candidates from data taken in 2003 August. Top panel shows data at the DM of the pulsar, the lower panel shows the same for a DM of 125 cm^{-3} pc. Note that phase 1.0 is in the centre of the plot.

profile mid-point) and 81 that arrive late. If we take the rate between phases 0.18 and 0.78 in Fig. 5 as 'background' we estimate that no more than three pulses are false positives in each of the early and late phase windows. The early arriving giants have a mean flux density of 10.4 mJy, higher than the 7.5 mJy for the mean flux density of the late arrivals. The three strongest giants from the sample are part of the early group.

Fig. 6 shows the unbinned cumulative probability distribution of our giant pulses on a log–log plot. A Kolmogorov–Smirnov comparison of the early and late giants gives a 1 per cent probability that these are drawn from the same distribution. Accordingly, we have used a Bayesian approach (Wheatland 2004) to fit a power-law distribution to the early and late giants separately, and to the combined set of giant pulses. These best-fitting power laws are plotted in Fig. 6. To facilitate comparison with other pulsars we express these giant pulse intensity distributions in units of 20 times the average pulse flux $S_{20\times} = S_{\rm GP}/(20\langle S_{1.4\,\rm GHz}\rangle)$, as this is often taken as a threshold defining giant pulse emission. For PSR B0540−69 $20\langle S_{1.4\,\rm GHz}\rangle = 500$ μJy. With these units, the best-fitting cumulative probability intensity distributions are:

$$\begin{aligned}
&\text{(early) } f_{>} = 2.7\times10^{-4} S_{20\times}^{-1.5\pm0.2}\\
&\text{(late) } f_{>} = 1.4\times10^{-3} S_{20\times}^{-2.1\pm0.3}\\
&\text{(total) } f_{>} = 1.2\times10^{-3} S_{20\times}^{-1.8\pm0.2}.
\end{aligned} \quad (1)$$

The limited statistics and refractive variations imply a ∼20 per cent uncertainty in the normalizations. For comparison, the Crab pulsar giant pulses have $f_{>} = 6\times10^{-3} S_{20\times}^{-2.3}$ (at 0.8 GHz; Lundgren et al. 1995), while PSR B1937+21 shows giant pulses with $f_{>} = 1\times10^{-5} S_{20\times}^{-1.8}$ (at 1.4 GHz, Kinkhabwala & Thorsett 2000). Note that the giant pulse distributions in PSR B0540−69 show some evidence for a break to a flatter index for $S < 7$ mJy, but with a limited dynamic range it is difficult to quantify the significance of such a break. There is no evidence of a cut-off at large pulse amplitudes. As noted below there is some evidence for refractive interstellar scintillation modulation of both the integrated profile flux and the giant pulse rate. We do not have a sufficient signal-to-noise ratio to calibrate this modulation. It does not strongly affect the fitted pulse

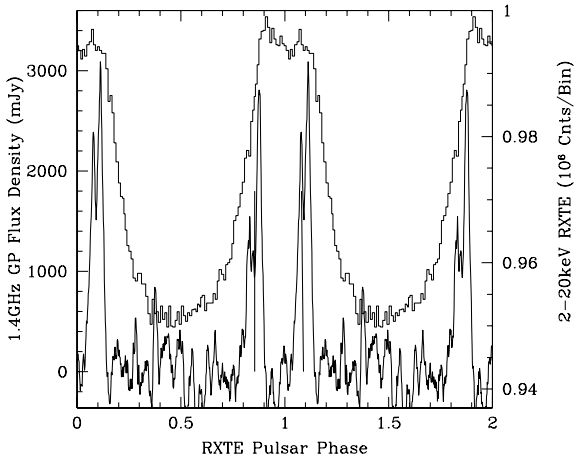

Figure 3. The sum of brightest 18 giant pulses from the 2003 August observations of PSR B0540−69 (thick line), compared with the *RXTE* light curve (thin line) taken from de Plaa et al. (2003). Note that phase 1.0 is in the centre of the plot.

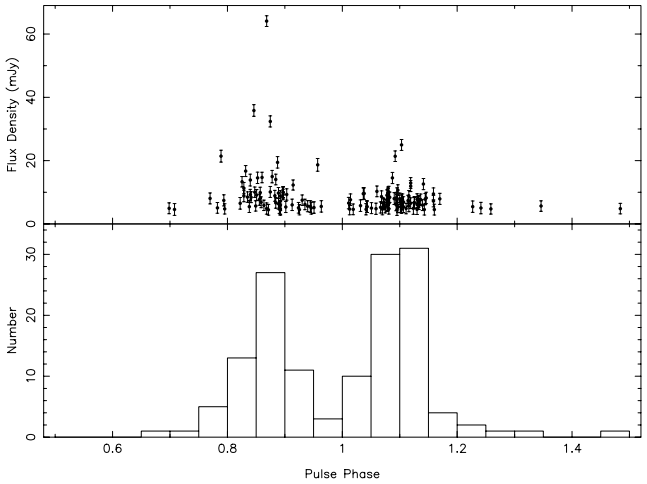

Figure 5. Top panel, location and flux density of the 141 giant pulse candidates obtained during 80 h of observing time. Bottom panel, histogram of the locations of the giant pulse candidates showing their division into two groups. Note that phase 1.0 is in the centre of the plot.

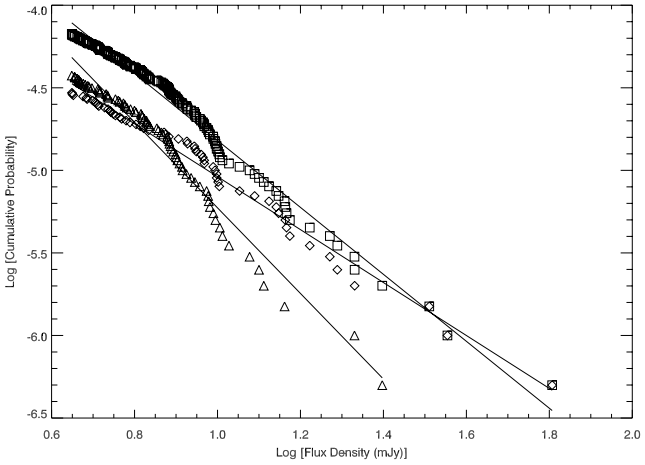

Figure 6. Cumulative log N – log S for the giant pulses. The 'early' giants are denoted by the diamonds, the 'late' giants by the triangles and the combined data set by the squares. A slope of -1.8 fits the full distribution. The 'early' giant pulses, however, show a shallower slope than the 'late' giant pulses and dominate the largest events.

distributions, although we note that largest two (early) giant pulses were seen at periods of low integrated flux. Correction for this effect would tend to further flatten the early giant pulse distribution.

The largest pulse (from the early group) has an equivalent continuum flux of 64 mJy, some 2500 times the mean flux and 3800 times the integrated flux density for this particular observing epoch. Overall, we obtain a $\gtrsim$10 mJy pulse every two hours, approximately equally from the two components. We expect one $\gtrsim$100 mJy pulse in $\sim$9 d of observing; this will probably occur from the early component.

5 INTEGRATED PROFILE OF PSR B0540−69

Armed with a timing solution we can now sum the data together to determine the integrated profile of PSR B0540−69. Fig. 7 shows the profile after summation of the data taken in 2003 August. The pulsar is clearly detected with an integrated flux density of 24 μJy. We also formed the integrated profile for each of the other observing sessions from 2003 and from 2001. With less integration time, the signal-to-noise ratio is not as good as in Fig. 7, but the flux densities we obtain are 16 μJy (2001), 19 μJy (2003 May/June) and 20 μJy (2003 September). We note that the variability in these values is consistent with the giant pulse rate, which also varies slightly from session to session. There is therefore some evidence for variability in the flux density with a modulation index of 0.15, probably due to refractive scintillation effects where the expected time-scale is of the order of days. Given the 640-MHz flux density quoted by Manchester et al. (1993), the radio spectral index of the integrated emission between 640 and 1390 MHz is -3.6, one of the steepest of all the known pulsars. In the Crab pulsar, the main pulse has a spectral index of -3.0, however, this spectral index is a mixture of the 'normal' radio emission, which probably has a steeper spectrum again, and the flatter spectrum giant pulse emission (Sallmen et al. 1999).

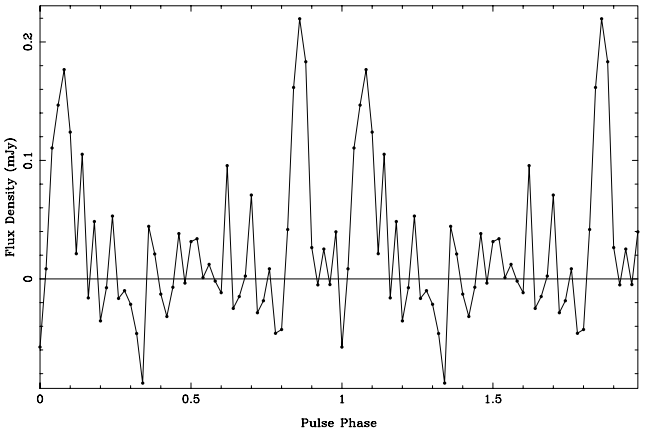

Figure 7. Integrated profile of PSR B0540−69 at 1.4 GHz from observations taken in 2003 August. Total time on-source was 31.2 h. There are 50 bins across the pulse phase for a resolution of $\sim$1 ms. The rms is 33 μJy.

The integrated profile looks similar to the 'giant profile' shown in Fig. 3, with a peak ratio similar to that seen in our set of early and late giants. However, the individual giants that we detect above threshold contribute only 0.2 μJy per pulse or less than 1 per cent of the integrated flux density. One may ask whether or not a population of subthreshold giants makes up most of the integrated profile (as for the Crab pulsar main and interpulse above 800 MHz; Lundgren et al. 1995) or whether or not the integrated profile is dominated by a 'normal' pulse population with an approximately Gaussian intensity distribution, as for PSR B1937+21, where the giant pulse emission is less than 1 per cent of the total (Kinkhabwala & Thorsett 2000; Jenet, Anderson & Prince 2001).

A cumulative giant pulse number distribution $f_> = As^\alpha$ contributes a flux $\langle s \rangle = \alpha\, A\, s_0^{(\alpha+1)}/(\alpha+1)$ above some cut-off s_0. For our intensity distributions above, even if every early pulse was drawn from the giant distribution (down to a threshold of 2 μJy), the giant pulses would only account for half of the first component flux. The late component could, in principal, be made up of giant pulses representing 10 per cent of the pulses, with a flux threshold of $\sim$65 μJy $\approx$ 2.5 $\langle s \rangle$. Given the similarity in the number of early and late giants above our observation threshold this seems rather unlikely. Instead, it seems more likely that only a modest fraction of the pulses are giants as for the Crab pulsar and PSR B1937+214. If we adopt a giant pulse fraction of 10^{-3}, then the flux threshold for a giant pulse in the early component is 200 μJy and these contribute 0.6 μJy or 5 per cent of the early component flux. The equivalent numbers for the late component give a threshold of $\sim$600 μJy and an integrated flux of 1.1 μJy, or $\sim$10 per cent of the late component flux. This would imply that both components are dominated by a conventional pulse distribution. Given the low flux, this will be difficult to confirm.

6 RADIO AND X-RAY COMPARISON

Although we have made several attempts to coordinate Parkes and *RXTE* observations, and have obtained several near-simultaneous epochs, only a modest amount of integration was simultaneous during the 2003 campaign. However, three giant radio pulses were obtained during an *RXTE* exposure on 2003 August 6 ($\sim$MJD 528 57.9) and two were observed on 2003 September 28 ($\sim$MJD 529 10.6). Examination of the X-ray data stream during these large ($\gtrsim$ 10 mJy) pulses allows an initial search for a high-energy excess. We have coadded the X-ray events surrounding the infinite frequency barycentric arrival time of these pulses. We have examined the *RXTE* light curve on a range of time-scales, finding no excess counts associated with the radio giant pulses.

We base our fiducial limit on the 5 × 5 ms time intervals centred on the giant pulses. The number of events expected from background, including diffuse X-rays, unrejected cosmic rays, X-rays from nearby sources that are in the collimated field of view, and

regular pulses from the pulsar, is estimated to be 2.1 in these 25 ms. As only four events are observed during these five windows, there is no statistically significant excess that can be associated with the giant pulses. Using Poisson statistics, we calculate that at the 90 per cent (99.5 per cent) confidence level the actual excess in coincidence with giant radio pulses is no more than 6.0 (10.6) events. In comparison, the phase-averaged X-ray pulse rate produces 0.084 counts in the interval. In other words, at the 90 per cent confidence level, any giant X-ray pulses associated with the radio giant pulses are no larger than 71 times the normal pulses.

However, considering that these detected radio giants represent an average excess of 400 times the mean radio emission, it is interesting to note that the X-ray enhancement is constrained to be 5.5 times smaller than that in the radio band. These results are consistent with other comparisons of high-energy fluctuations with radio giant pulse emission as detailed in the introduction. It is evident that the factors of 1000 or more seen in the differences between the giant pulse emission and the normal emission in the radio are not observed at higher energies.

The limits on the high-energy pulse modulation and the rather small claimed enhancement on the optical flux associated with radio giant pulse events certainly suggest that giant pulses are caused by coherence fluctuations rather than changes in total plasma density. Accordingly, it is intriguing that the giant pulse phenomenon appears to be associated with the light cylinder field rather than the surface dipole. This might suggest that growing instabilities (e.g. two-stream or radiation back-reaction) in plasma flowing through the outer magnetosphere mediate the radio giant pulse modulations, and that the longer path-length in this zone allows larger fluctuation amplitudes.

PSR B0540−69 also apparently follows the Crab pulsar and the millisecond pulsars PSR B1937+21 and B1821–24 in having the giant pulse emission confined to phases that also show narrow, hard-spectrum X-ray components. Better statistics and improved relative timing might show that the giant pulse events are associated with the peak structure in the X-ray pulse of PSR B0540−69, which would further strengthen this conclusion.

If we take this connection with the outer magnetosphere and with the hard X-ray emission seriously, we should ask how this relates to the expected pulse structure of high-energy emission models. Both the outer gap picture described by Romani & Yadigaroglu (1995) and the two-pole (extended slot gap) picture of Dyks, Harding & Rudak (2004) give loci for narrow pulse components far from the star surface that lie off the magnetic pole. At present, the best clue we have to the emission geometry in PSR B0540−69 is the 0.25 phase separation of the giant pulse components. Such separations are naturally seen in the outer gap picture for viewing angle $\zeta \leqslant 75^\circ$. This may, however, be in disagreement with the X-ray torus of wind nebula around PSR B0540−69 as measured by the *Chandra* X-ray Observatory (Gotthelf & Wang 2000), which appears to be closer to edge-on $\zeta \approx 85^\circ$. It is not clear if the two-pole models can give such narrow pulse separations for any angles. Certainly independent measurement of the viewing geometry would help greatly in constraining the location of the giant pulse emission regions. Unfortunately, radio polarization measurements to test the viewing angles will be difficult to obtain for this pulsar; the position angle sweep may, however, be measurable in the optical band.

7 CONCLUSIONS

We have carried out extensive observations of PSR B0540−69 at radio wavelengths and have also obtained simultaneous radio and X-ray observations of the pulsar. The observations have enabled us to determine that the giant pulses in the radio arrive in-phase with the X-ray pulses. However, we see no enhancement in the X-ray flux at the time of the radio giants. We have shown that the giant pulses follow power-law statistics. It seems likely that they contribute only a few per cent to the integrated flux density. All four pulsars that are giant pulse emitters (two young pulsars and two millisecond pulsars) show similar characteristics.

ACKNOWLEDGMENTS

RWR is supported in part by NASA grant NAS-13344. The Australia Telescope is funded by the Commonwealth of Australia for operation as a National Facility managed by the CSIRO. We thank J. Reynolds for providing unallocated telescope time for this project and A. Karastergiou and S. Ord for help with observing.

REFERENCES

Caraveo P. A., Bignami G. F., Mereghetti S., Mombelli M., 1992, ApJ, 395, L103
Cusumano G., Massaro E., Mineo T., 2003a, A&A, 402, 647
Cusumano G. et al., 2003b, A&A, 410, L9
de Plaa J., Kuiper L., Hermsen W., 2003, A&A, 400, 1013
Dyks J., Harding A. K., Rudak B. 2004, ApJ, 606, 1125
Gotthelf E. V., Wang Q. D., 2000, ApJ, 532, L117
Jenet F. A., Anderson S. B., Prince T. A., 2001, ApJ, 546, 394
Johnston S., Romani R., 2003, ApJ, 590, L95 (Paper I)
Kinkhabwala A., Thorsett S. E., 2000, ApJ, 535, 365
Lundgren S. C., Cordes J. M., Ulmer M., Matz S. M., Lomatch S., Foster R. S., Hankins T., 1995, ApJ, 453, 433
Manchester R. N., Mar D., Lyne A. G., Kaspi V. M., Johnston S., 1993, ApJ, 403, L29
Romani R., Johnston S., 2001, ApJ, 557, L93
Romani R. W., Yadigaroglu I.-A., 1995, ApJ, 438, 314
Sallmen S., Backer D. C., Hankins T. H., Moffett D., Lundgren S., 1999, ApJ, 517, 460
Seward F. D., Harnden F. R., Helfand D. J., 1984, ApJ, 287, L19
Shearer A., Stappers B., O'Connor P., Golden A., Strom R., Redfern M., Ryan O., 2003, Sci, 301, 493
Vivekanand M., 2001a, A&A, 373, 236
Vivekanand M., 2001b, A&A, 376, 580
Wheatland M. S., 2004, ApJ, 609, 1134
Zhang W., Marshall F. E., Gotthelf E. V., Middleditch J., Wang Q. D., 2001, ApJ, 554, L177

This paper has been typeset from a TEX/LATEX file prepared by the author.